JACS
JOURNAL OF THE AMERICAN CHEMICAL SOCIETY
Article
pubs.acs.org/JACS

Functional Model for the [Fe] Hydrogenase Inspired by the Frustrated Lewis Pair Concept

Kai F. Kalz,[†] Alexander Brinkmeier,[†] Sebastian Dechert,[†] Ricardo A. Mata,[‡] and Franc Meyer*[,†]

[†]Institute of Inorganic Chemistry, Georg-August-University Göttingen, Tammannstrasse 4, D-37077 Göttingen, Germany
[‡]Institute of Physical Chemistry, Georg-August-University Göttingen, Tammannstrasse 6, D-37077 Göttingen, Germany

Supporting Information

ABSTRACT: [Fe] hydrogenase (Hmd) catalyzes the heterolytic splitting of H_2 by using, in its active site, a unique organometallic iron-guanylylpyridinol (FeGP) cofactor and, as a hydride acceptor, the substrate methenyltetrahydromethanopterin (methenyl-H_4MPT$^+$). The combination FeGP/methenyl-H_4MPT$^+$ and its reactivity bear resemblance to the concept of frustrated Lewis pairs (FLPs), some of which have been shown to heterolytically activate H_2. The present work exploits this interpretation of Hmd reactivity by using the combination of Lewis basic ruthenium metalates, namely K[CpRu(CO)$_2$] (**KRp**) and a related polymeric Cp/Ru/CO compound (**Rs**), with the new imidazolinium salt 1,3-bis(2,6-difluorophenyl)-2-(4-tolyl)imidazolinium bromide ([^{Tol}Im^{F4}]$^+$Br$^-$) that was designed to emulate the hydride acceptor properties of methenyl-H_4MPT$^+$. Solid-state structures of [^{Tol}Im^{F4}]$^+$Br$^-$ and the corresponding imidazolidine H^{Tol}Im^{F4} reveal that the heterocycle undergoes similar structural changes as in the biological substrate. DFT calculations indicate that heterolytic splitting of dihydrogen by the FLP Rp$^-$/[^{Tol}Im^{F4}]$^+$ is exothermic, but the formation of the initial Lewis pair should be unfavorable in polar solvents. Consequently the combination Rp$^-$/[^{Tol}Im^{F4}]$^+$ does not react with H_2 but leads instead to side products from nucleophilic substitution ($k = 4 \times 10^{-2}$ L mol^{-1} s^{-1} at room temperature). In contrast, the heterogeneous combination Rs/[^{Tol}Im^{F4}]$^+$ does split H_2 heterolytically to give H^{Tol}Im^{F4} and HRuCp(CO)$_2$ (**HRp**) or D^{Tol}Im^{F4} and **DRp** when using D_2. The reaction has been followed by ^{1}H/^{2}H and ^{19}F NMR spectroscopy as well as by IR spectroscopy and reaches 96% conversion after 1 d. Formation of H^{Tol}Im^{F4} under these conditions demonstrates that superelectrophilic activation by protonation, which has been proposed for methenyl-H_4MPT$^+$ to increase its carbocationic character, is not necessarily required for an imidazolinium ion to serve as a hydride acceptor. This unprecedented functional model for the [Fe] hydrogenase, using a Lewis acidic imidazolinium salt as a biomimetic hydride acceptor in combination with an organometallic Lewis base, may provide new inspiration for biomimetic H_2 activation.

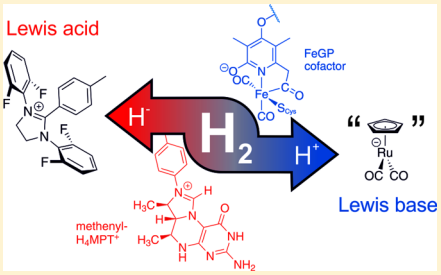

INTRODUCTION

In view of the world's ever increasing demand for energy, and powered by the search for a sustainable energy supply, dihydrogen is seen among the promising energy carriers of the future.[1,2] However, the efficient production, storage, and splitting of dihydrogen still poses a significant challenge. Nature provides valuable inspiration for the development of H_2 formation and activation catalysts as embodied by a unique class of metalloenzymes called hydrogenases, which efficiently catalyze the reversible formation and heterolytic cleavage of H_2.[3−7] Well-known and extensively characterized are the binuclear [FeFe] and [NiFe] hydrogenases,[7−11] for which a large body of biomimetic model complexes has been developed.[12−16] A third phylogenetically unrelated type, the [Fe] hydrogenase (Hmd), has been discovered more recently and has attracted wider attention only in the past few years.[17−20] While [Fe] hydrogenase was initially thought to be a purely organic hydrogenation catalyst,[21,22] subsequent investigations revealed a unique mononuclear iron-guanylylpyridinol (FeGP) cofactor.[23,24] As in the other hydrogenases it features an Fe^{II}(CO) moiety, but in [Fe] hydrogenase this is bound to one cysteine sulfur atom, an sp^2-hybridized pyridine nitrogen atom and an acyl carbon atom, thus representing a rather unusual organometallic binding motif in biological systems.[25] In many methanogenic archea, [Fe] hydrogenase catalyzes the reversible reduction of methenyltetrahydromethanopterin (methenyl-H_4MPT$^+$) to methylenetetrahydromethanopterin (methylene-H_4MPT), thereby splitting the H_2 molecule heterolytically and transferring a hydride ion stereospecifically to the *pro-R* site of the acceptor molecule (Scheme 1).[26]

Since the crystallographic elucidation of the [Fe] hydrogenase active site,[23,24] great efforts have been devoted to emulating the unusual iron-acyl ligation in structural model complexes,[7,20,27−35] and computational work has addressed possible reaction mechanisms.[36−41] But despite all the progress made, to our knowledge no functional synthetic analogue that mimics [Fe] hydrogenase reactivity has been developed up to now. Such a functional model might not only provide experimental insight into the enzyme's mechanism but could also delineate new avenues for hydrogen activation in artificial

Received: September 5, 2014
Published: October 29, 2014

   dx.doi.org/10.1021/ja509186d | J. Am. Chem. Soc. 2014, 136, 16626−16634

Scheme 1. Reversible Reduction of Methenyl-H_4MPT$^+$ to Methylene-H_4MPT by [Fe] Hydrogenase

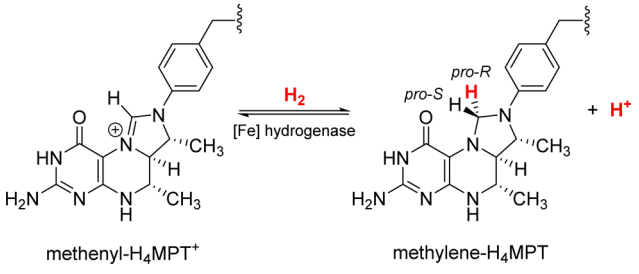

catalysts. A major obstacle so far has been the lack of a suitable model substrate for the methenyl-H_4MPT$^+$ hydride acceptor.

From a chemical point of view, methenyl-H_4MPT$^+$ serves as a Lewis acid to take up a hydride, while the FeGP cofactor represents a base that becomes protonated. This situation brings to mind the concept of frustrated Lewis pairs (FLPs), which has led to an important class of new H_2 activation catalysts during the past decade.[42] Certain FLPs, pioneered by Stephan and Erker,[43,44] utilize the strain that is inherent to—mainly transition-metal-free—pairs of sterically encumbered Lewis acids and bases to cleave H_2. Especially the FLP systems using an N-heterocyclic carbene as base, developed simultaneously in the groups of Tamm and Stephan (Figure 1, top),[45,46] prompted us to design a novel FLP system reminiscent of the [Fe] hydrogenase active site, where now an imidazolinium-based Lewis acid works in concert with a Lewis basic carbonylmetalate, for example, the ruthenium metalate $[CpRu(CO)_2]^-$ (**Rp**$^-$), in order to activate the H_2 molecule (Figure 1, bottom). The Ru-based metalate K[$CpRu(CO)_2$] (**KRp**) was chosen instead of Fe-based anionic carbonylmetalates, since $HRuCp(CO)_2$ (**HRp**) is less acidic (pK_a 28.3), has a higher M−H bond dissociation free energy (72 kcal/mol), and is less prone to degradation to dimeric $[CpRu(CO)_2]_2$ (**Rp$_2$**) compared to its congener $HFeCp(CO)_2$ (**HFp**).[47] Preliminary experiments, probing reactions between various imidazolinium salts and the carbonylferrate **KFp**, indeed showed undesired side reactions, likely involving single electron transfer (SET) reactions (see Supporting Information).

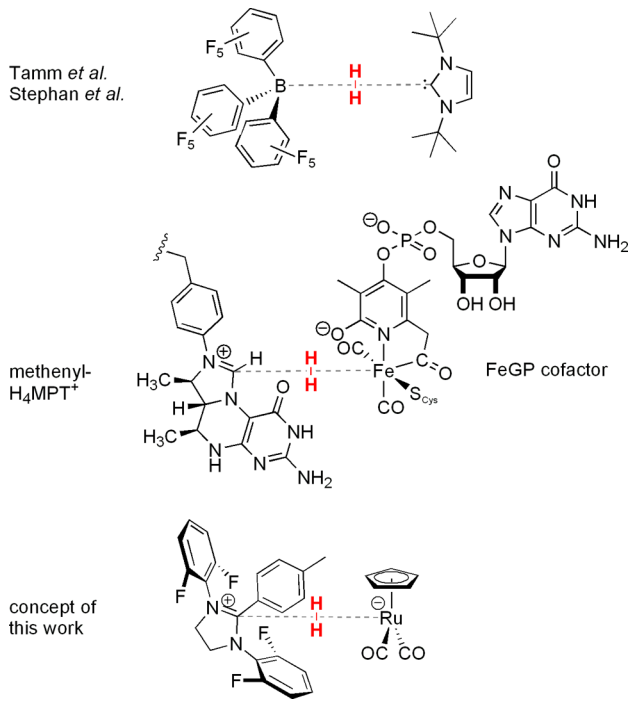

Figure 1. Comparison between a carbene FLP (top),[45,46] the active site of [Fe] hydrogenase (middle), and the envisioned system in this work (bottom).

For the Lewis acid part our approach thus required the development of a new imidazolium salt suited for serving as a methenyl-H_4MPT$^+$ model substrate. With respect to the Lewis base side, we recently reported a revised protocol for the synthesis of **KRp** via reductive cleavage of (**Rp$_2$**), which allowed for the isolating of **KRp** in crystalline form in about 40% yield.[48] Further we found that the reductive cleavage of **Rp$_2$** also produced, as a second product, a poorly soluble black solid (**Rs**). Thorough investigation of this material by a variety of methods, including ^{13}C MAS NMR spectroscopy using ^{13}CO-labeled material,[48] led us to conclude that it consisted of a presumably polymeric Cp/Ru/CO compound in which the "$CpRu(CO)_2$" unit is in some way conserved, but with both bridging and terminal CO ligands in a 3:1 ratio.[48] Both the monomeric **KRp** and the polymeric Cp/Ru/CO compound **Rs** can be protonated at the metal center to yield the corresponding hydride complex, **HRp**. Consequently, two different ruthenium metalates, viz. **KRp** and **Rs**, are now available for use in the present context.

In this contribution we report our attempts to utilize these ruthenium metalates, molecular **KRp** and polymeric **Rs**, in combination with a well-designed imidazolinium ion to mimic the natural [Fe] hydrogenase in terms of its proton-accepting metal unit as well as its hydride acceptor molecule methenyl-H_4MPT$^+$. Such a system would be one of the rare examples for FLP reactivity without boron-containing Lewis acids and the first to use an imidazolinium ion akin to methenyl-H_4MPT$^+$ as the Lewis acid. Conceptually related to recently reported metal−borane complexes,[49−55] the envisioned system would also be the first with a transition-metal compound acting as a Lewis base in a "real" FLP, complementing recent examples of FLP systems that feature transition metals as Lewis acids.[56−59] It should finally be noted that recent quantum mechanics/molecular mechanics (QM/MM) calculations on snapshots of the H_2 activation in [Fe] hydrogenase by Reiher et al.[41] indeed suggested a metal-mediated mechanism reminiscent of H_2 activation by frustrated Lewis pairs, though using the deprotonated pyridinol as a base.

RESULTS AND DISCUSSION

Design of the Hydride Acceptor Molecule. In order to find a suitable hydride acceptor molecule that is structurally related to methenyl-H_4MPT$^+$, a variety of imidazolinium salts was synthesized and screened with respect to their hydride accepting ability in a test reaction with $NaBH_4$; three selected examples are shown in Figure 2. Contrary to methenyl-H_4MPT$^+$, the imidazolinium ions were equipped with bulky residues at the C-2 positions of the heterocycle to prevent deprotonation and carbene formation or formation of simple Lewis acid/base adducts upon treatment with the basic metalate.

While many screened imidazolinium salts such as $[^{Tol}Im^{Mes}]^+Br^-$ did not react with $NaBH_4$ to give the corresponding imidazolidine, best results were obtained with derivatives having N-aryl substituents with electron-withdrawing fluoride substituents, likely because of increased

dx.doi.org/10.1021/ja509186d | J. Am. Chem. Soc. 2014, 136, 16626−16634

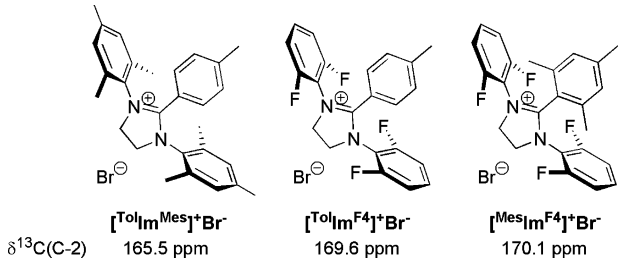

Figure 2. Selected imidazolinium salts synthesized and screened in this work, including the most favorable derivative $[^{Tol}\mathbf{Im}^{F4}]^{+}\mathbf{Br}^{-}$; and ^{13}C NMR chemical shift of the C-2 atoms (in $CDCl_3$).

hydricity of the C-2 atom. The hydricity can be estimated based on the ^{13}C NMR chemical shift of the C-2 atom (see Figure 2), but steric constraints also play a role, e.g., the bulky mesityl group in $[^{Mes}\mathbf{Im}^{F4}]^{+}\mathbf{Br}^{-}$ prevents pyramidalization at C-2 and thus impedes hydride addition. 1,3-Bis(2,6-difluorophenyl)-2-(4-tolyl)imidazolinium bromide ($[^{Tol}\mathbf{Im}^{F4}]^{+}\mathbf{Br}^{-}$) finally met all requirements and furthermore showed reduced sensitivity toward nucleophilic attack by $\mathbf{Rp}^{-}$ at the *para*-position of the phenyl substituents (which was identified as a possible side reaction). As an added value it allows the use of ^{19}F NMR spectroscopy as a convenient probe for monitoring the reaction progress (see below).

Figure 3 shows a comparison between the solid-state structures of $[^{Tol}\mathbf{Im}^{F4}]^{+}\mathbf{Br}^{-}$ and the corresponding imidazolidine ($\mathbf{H}^{Tol}\mathbf{Im}^{F4}$) obtained after reaction with $NaBH_4$ in EtOH at room temperature. From the crystallographic data it is evident that the almost planar imidazolinium heterocycle in $[^{Tol}\mathbf{Im}^{F4}]^{+}\mathbf{Br}^{-}$ undergoes severe structural changes upon accepting a hydride ion. In the solid state, $\mathbf{H}^{Tol}\mathbf{Im}^{F4}$ adopts an envelope conformation with one carbon atom being located above (0.6 Å) the plane defined by both N atoms and the C-2 carbon atom. Imposing some non-planarity to an imidazolium ion may be a key for enhancing its hydride acceptor ability in future improved model systems. The envelope conformation found for $\mathbf{H}^{Tol}\mathbf{Im}^{F4}$ parallels to some extent what was found for the structure of an enzyme–substrate complex, where the reduced methylene-H_4MPT is bound to the open form of the enzyme (Figure 3).[26] However, in the enzyme–substrate complex, the imidazolidine ring is slightly more planar since the dislocated carbon atom is only 0.4 Å above the plane through both nitrogen atoms (N^5 and N^{10}) and the central carbon atom (C^{14a}; atom labeling according to ref 26).

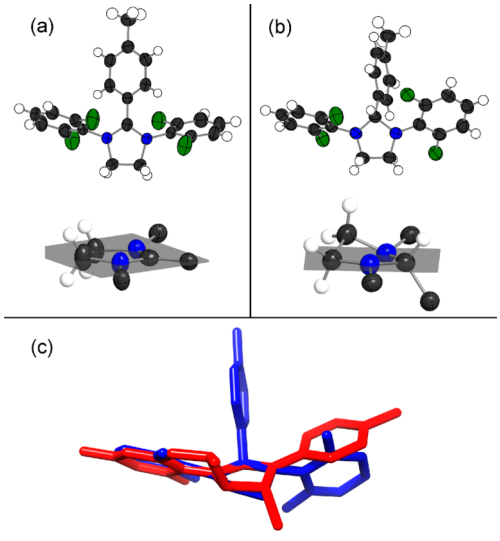

Figure 3. Comparison between the solid-state structures of (a) $[^{Tol}\mathbf{Im}^{F4}]^{+}\mathbf{Br}^{-}$ and (b) $\mathbf{H}^{Tol}\mathbf{Im}^{F4}$ and (c) superposition of $\mathbf{H}^{Tol}\mathbf{Im}^{F4}$ (blue) and methylene-H_4MPT found in the crystal structure of the enzyme–substrate complex (red, atoms beyond the phenyl ring are omitted).[26]

Furthermore, the orientation of the N-bound substituents differs. These differences may be related to the annulated ring system in methylene-H_4MPT and/or the protein environment imposing a more planar conformation on the imidazolidine ring, thereby facilitating hydride transfer in the natural system by minimizing structural changes during the reaction.[60]

Theoretical Calculations. DFT calculations were performed to assess the thermodynamics of heterolytic H_2 splitting by the FLP-like combination of $\mathbf{Rp}^{-}$ and $[^{Tol}\mathbf{Im}^{F4}]^{+}$ to give **HRp** and $\mathbf{H}^{Tol}\mathbf{Im}^{F4}$. For this purpose, possible intermediates and transitions states were optimized at the B3LYP-D3/def2-TZVP level of theory.[61,62] The calculations included a COSMO correction for the solvent MeCN[63] and the energy recomputed with the def2-QZVPP basis set.[62] Free energy estimates were obtained on the basis of the unscaled harmonic vibrational spectra (B3LYP-D3/def2-TZVP) of the optimized stationary points. Thermal corrections were calculated using the rigid rotor/harmonic oscillator model. In order to correct for the typical overestimation of entropic factors in solution along a pathway in which the number of molecular units is changing, the cell model proposed by Ardura et al.[64] was applied. The latter is added as a correction to the gas phase entropies, which are computed under the ideal gas approximation. Due to the poor treatment of translational degrees of freedom in solution, this can otherwise result in large free energy penalties for complex formation.[65] Further details on the performed calculations are provided in the Experimental Section.

The obtained reaction path is depicted in Figure 4. Initially, a Lewis pair with a close contact between the Ru atom of the metalate and the C-2 carbon atom of $[^{Tol}\mathbf{Im}^{F4}]^{+}$ is formed. This process is endothermic and associated with a free energy penalty of 55.5 kJ mol^{-1} which indicates that any formation of the Lewis pair is rather unlikely in MeCN solution. However, the computed value is highly dependent on the solution environment since the performed B3LYP-COSMO correction contributes more than 300 kJ mol^{-1} to the final energy. This is to be expected since one is calculating the formation of an uncharged Lewis pair from two charged compounds. The effect of a polar environment will be determinant for the stability of such a structure. With an increasing dielectric constant, charge separation will be favored, and the dimer formation becomes less likely. Given the approximations made to describe this effect, this result should be regarded with caution. Nevertheless, the relative energies between the following species of the reaction path are considerably less affected by the COSMO corrections and are more reliable in this respect; the latter are about an order of magnitude lower than those found for the Lewis pair formation. As it can be observed in Figure 4, the dihydrogen complex (reactant complex, RC) is stable relative to the frustrated Lewis pair (by about 10.3 kJ mol^{-1}). The actual reaction barrier is relatively small (26.4 kJ mol^{-1}), and therefore a heterolytic splitting of H_2 by this system should be possible, as long as a contact is established between the two reaction centers. The product complex (PC) is much more stable, and it

dx.doi.org/10.1021/ja509186d | J. Am. Chem. Soc. 2014, 136, 16626–16634

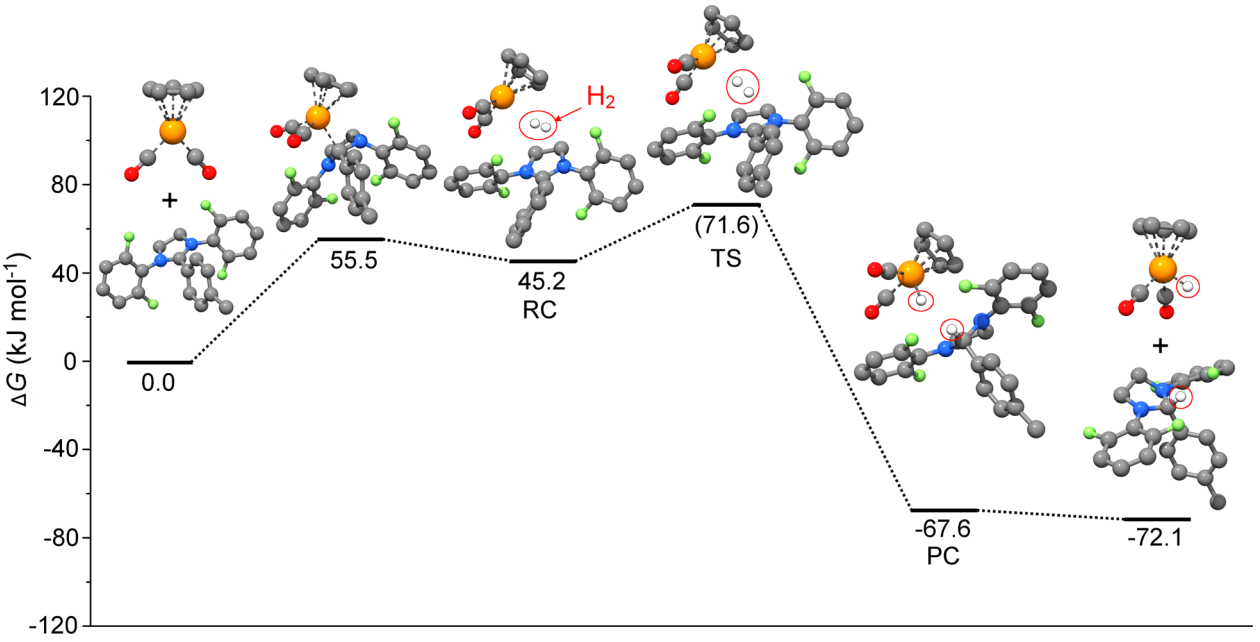

Figure 4. Calculated reaction path for the heterolytic splitting of H_2 by an FLP consisting of the $\mathbf{Rp}^-$ and $[^{Tol}\mathbf{Im}^{F4}]^+$ ions.

could readily dissociate in solution to the final products **HRp** and $\mathbf{H}^{Tol}\mathbf{Im}^{F4}$.

The TS structure was obtained by scanning a large number of different conformations of the Lewis pair with a smaller basis (def2-SVP). This was necessary due to the high dimensionality of the system and the inherent difficulty in obtaining a connected reaction path. The energy for this state is estimated from the height of the obtained reaction curve (relative to RC). The procedure used is described in the Experimental Section. In summary, the computational results indicate that heterolytic splitting of dihydrogen by the FLP $\mathbf{Rp}^-/[^{Tol}\mathbf{Im}^{F4}]^+$ is exothermic. However, the major obstacle for achieving H_2 dissociation is the formation of the Lewis pair from the isolated ions $\mathbf{Rp}^-$ and $[^{Tol}\mathbf{Im}^{F4}]^+$. We surmised that this problem may be circumvented by using the insoluble Cp/Ru/CO compound **Rs**. Unfortunately, no such calculations can be performed for the combination $\mathbf{Rs}/[^{Tol}\mathbf{Im}^{F4}]^+$, because of the ill-defined nature of polymeric **Rs**. At least the above calculations show that once the products **HRp** and $\mathbf{H}^{Tol}\mathbf{Im}^{F4}$ are formed, they should be thermodynamically stable with respect to the reverse reaction, the liberation of H_2.

The Combination $\mathbf{Rp}^-/[^{Tol}\mathbf{Im}^{F4}]^+$. In order to obtain the desired (frustrated) Lewis pair, a salt metathesis reaction using the imidazolinium salt $[^{Tol}\mathbf{Im}^{F4}]^+\mathbf{Br}^-$ and **KRp** was performed. However, mixing the imidazolinium salt and the metalate **KRp** dissolved in MeCN did not yield the anticipated FLP but led to a reaction between both components. Reaction monitoring by IR spectroscopy showed a gradual decrease of the CO bands of the $\mathbf{Rp}^-$ anion at 1887 and 1802 cm^{-1} and concomitant rise of new bands at 2034 and 1971 cm^{-1}, the latter representing a new dicarbonyl species. Besides this, small amounts of the dimer $\mathbf{Rp}_2$ ($\tilde{\nu}$ = 1996, 1775 cm^{-1}) were detected in solution. Kinetic analysis of the reaction by quantifying the peak area of the $\tilde{\nu}$(CO) bands gave a rate constant of $k = 4 \times 10^{-2}$ L mol^{-1} s^{-1} at room temperature in the initial stages of the bimolecular reaction (see Supporting Information). Crystals of the product suitable for X-ray crystallography could be obtained from a mixture of MeCN and toluene. The molecular structure determined by X-ray diffraction confirmed that the reaction product ($[\mathbf{Rp}^{Tol}\mathbf{Im}^{F3}]^+\mathbf{Br}^-$) originated from the nucleophilic substitution of one of the four fluorine atoms of the imidazolinium ion by the metalate $\mathbf{Rp}^-$ (Figure 5).

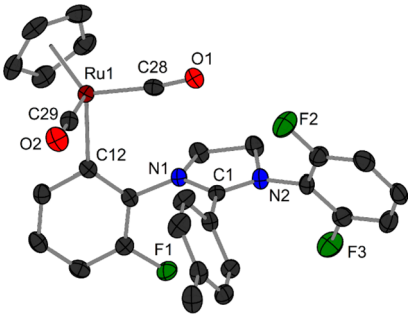

Figure 5. Molecular structure of the adduct $[\mathbf{Rp}^{Tol}\mathbf{Im}^{F3}]^+\mathbf{Br}^-$ formed after mixing **KRp** and $[^{Tol}\mathbf{Im}^{F4}]^+\mathbf{Br}^-$. Thermal displacement ellipsoids are given at 50% probability; hydrogen atoms, the bromide counteranion, and an additional MeCN molecule are omitted for clarity. Selected bond length [Å] and angles [°]: Ru1–C12 = 2.107(2), Ru1–C28 = 1.879(3), Ru1–C29 = 1.884(3), C28–O1 = 1.146(3), C29–O2 = 1.138(3), N1–C1 = 1.324(3), N2–C1 = 1.323(3), Ru1–C28–O1 = 173.0(2), Ru1–C29–O2 = 176.2(2), C29–Ru1–C28 = 94.5(1), C29–Ru1–C12 = 84.1(1), C28–Ru1–C12 = 97.4(1), N1–C1–N2 = 111.9(2).

The Combination $\mathbf{Rs}/[^{Tol}\mathbf{Im}^{F4}]^+$ and Hydrogen Splitting. Adding the polymeric Cp/Ru/CO material **Rs** to a solution of $[^{Tol}\mathbf{Im}^{F4}]^+\mathbf{Br}^-$ in CD_3CN did not lead to any reaction between the components, even after prolonged heating of the mixture to 50 °C.[66] When the mixture was exposed to H_2, however, heterolytic splitting of dihydrogen was observed. Figure 6 shows ^{1}H NMR spectra recorded at selected times after combining $[^{Tol}\mathbf{Im}^{F4}]^+\mathbf{Br}^-$, the black solid **Rs** and H_2 (8 bar) in CD_3CN at room temperature. From the ^{1}H NMR spectra it is evident that $[^{Tol}\mathbf{Im}^{F4}]^+\mathbf{Br}^-$ is consumed, while $\mathbf{H}^{Tol}\mathbf{Im}^{F4}$ is formed. The signal for the CH_2 groups of the starting material at 4.64 ppm decreases, and at the same time two multiplets corresponding to the diastereotopic CH_2

dx.doi.org/10.1021/ja509186d | J. Am. Chem. Soc. 2014, 136, 16626–16634

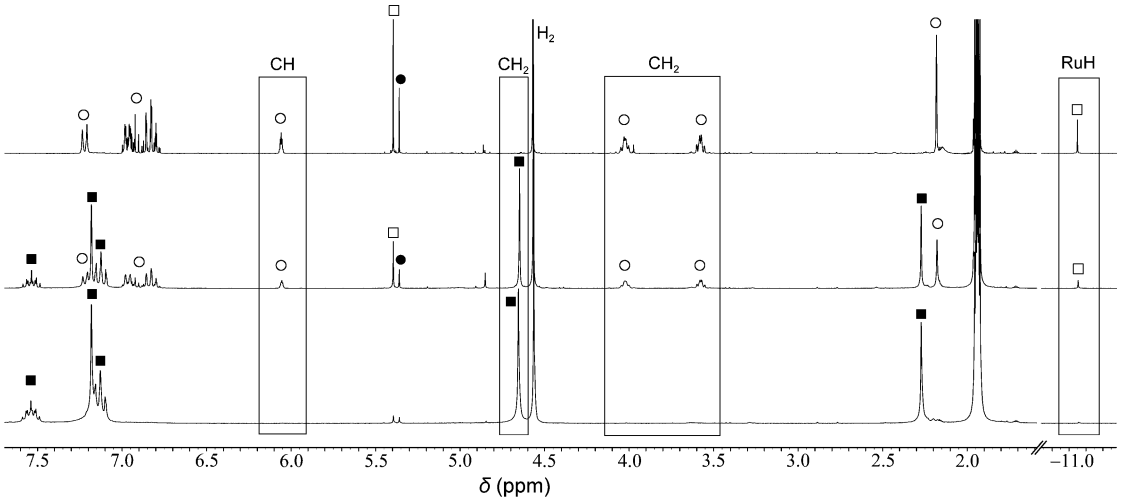

Figure 6. ^{1}H NMR spectra (300 MHz) of the mixture of $[^{Tol}Im^{F4}]^+Br^-$, **Rs**, and H_2 (8 bar) in CD_3CN at room temperature after 6 min, 1 h, and 3 d (bottom to top). Signals assigned to $[^{Tol}Im^{F4}]^+Br^-$ (■), $H^{Tol}Im^{F4}$ (○), **HRp** (□), and **Rp$_2$** (●) are marked with geometric symbols; CH, CH_2, and hydride regions are highlighted by frames. Detailed views of the time-dependent evolution of the different signals are provided in the Supporting Information.

protons of the product $H^{Tol}Im^{F4}$ at 4.05−4.00 and 3.60−3.55 ppm increase in intensity. Furthermore, new characteristic signals for the CH proton of $H^{Tol}Im^{F4}$ (6.06 ppm) and the hydride of **HRp** at −11.05 ppm arise. These signals clearly originate from the uptake of a hydride ion at the C-2 position of the imidazolinium ion and from protonation of the metalate. Hence a heterolytic splitting of H_2 has taken place. The spectra show no signals for the polymeric black material **Rs** because of its poor solubility under the applied conditions. Integration of the CH signal of $H^{Tol}Im^{F4}$ and the H−Ru signal does not show the expected 1:1 ratio, but the concentration of the metal hydride **HRp** seems to be constantly too low. One possible reason accounting for this is the partial decomposition of the formed **HRp** to dimeric **Rp$_2$**, which is indeed discernible in the ^{1}H NMR spectrum (Figure 6).

To confirm that both the CH in $H^{Tol}Im^{F4}$ and the Ru−H originate from H_2, the reaction was also carried out with D_2. Heterolytic cleavage of D_2 was indeed observed, evidenced by characteristic ^{2}H NMR resonances for the deuterated compounds $D^{Tol}Im^{F4}$ and **DRp** (see Supporting Information); these can be found at roughly the same chemical shifts as for $H^{Tol}Im^{F4}$ and **HRp** in the corresponding ^{1}H NMR spectrum. The identity of $D^{Tol}Im^{F4}$ was further confirmed by its independent synthesis from $[^{Tol}Im^{F4}]^+Br^-$ and $NaBD_4$. Further proof for the formation of $H^{Tol}Im^{F4}$ and **HRp** during the reaction of **Rs**/$[^{Tol}Im^{F4}]^+$ with H_2 came from IR spectroscopy in solution (CD_3CN). In the IR spectrum of the reaction mixture (see Supporting Information) characteristic bands for vibrations of the ruthenium hydride **HRp** at 2025 and 1960 cm^{-1} (antisymmetric and symmetric CO stretches)[47,67,68] and for the imidazolidine $H^{Tol}Im^{F4}$ evolve. At the same time all characteristic vibrations for the imidazolinium ion $[^{Tol}Im^{F4}]^+Br^-$ disappear. When in a control experiment a suspension of only the solid Cp/Ru/CO material **Rs** in CD_3CN was left under H_2 (8 bar) at room temperature, slow H/D exchange was observed (H_2/HD ratio 1:4 after 12 d, 1:6 after 47 d); similarly slow HD formation was observed for a suspension of **Rs** in CH_3CN under D_2 (8 bar). It can thus be assumed that H_2 activation occurs at the Cp/Ru/CO material **Rs**. While atomic-scale details of this H_2 activation mode are unknown at present, it is evident that in the presence of $[^{Tol}Im^{F4}]^+$ a hydride is transferred to the Lewis acidic imidazolinium ion that emulates the methenyl-H_4MPT$^+$ hydride acceptor of the [Fe] hydrogenase. The time dependence of this reaction was followed by ^{19}F NMR spectroscopy which shows the vanishing resonance for $[^{Tol}Im^{F4}]^+$ and the emerging resonance for $H^{Tol}Im^{F4}$ as the sole signals (Figure 7).

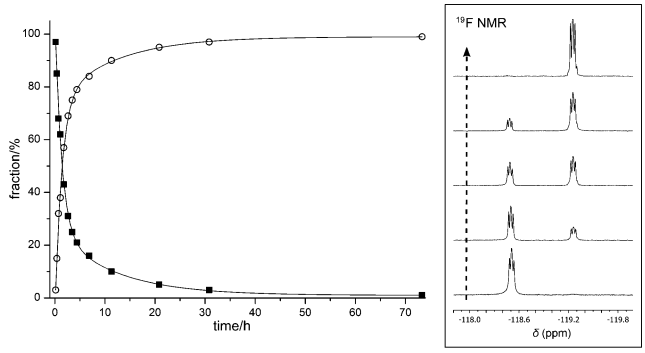

Figure 7. Time dependence of the composition of the reaction mixture followed by ^{19}F NMR spectroscopy; see Experimental Section for reaction conditions. The signal for $[^{Tol}Im^{F4}]^+Br^-$ (■) at −118.5 ppm decreases while the signal for $H^{Tol}Im^{F4}$ (○) at −119.3 ppm increases over time.

From the ratio of the integrals it becomes clear that, under the specific reaction conditions (see Experimental Section), the reaction is almost complete after 1 d (96% conversion). However, the heterogeneous character of the sample unfortunately impeded any detailed kinetic analysis of the reaction so far.

■ CONCLUSIONS

In summary, we herein report the successful synthesis of the first functional model for the [Fe] hydrogenase active site, whose reactivity toward H_2 and D_2 has been elucidated by means of NMR and IR spectroscopy. Though not containing Fe but its heavier congener Ru, our model system emulates the heterolytic splitting of H_2 through the cooperative action of a

dx.doi.org/10.1021/ja509186d | J. Am. Chem. Soc. 2014, 136, 16626−16634

Lewis acidic imidazolinium ion, that serves as a hydride acceptor similar to methenyl-H_4MPT^+, and a Lewis basic metal complex accepting the proton (to generate $HRuCp(CO)_2$, **HRp**). In this picture the mechanism operative in [Fe] hydrogenase bears close resemblance to the heterolytic H_2 splitting by frustrated Lewis pairs. An Fe−H intermediate in the [Fe] hydrogenase mechanism has indeed been implicated in some computational studies, although such intermediate could not be detected by Mößbauer spectroscopy and was thus deemed unlikely as a long-lived species.[69] Instead it has mostly been proposed that a ligand in the Fe coordination sphere (cysteine thiolato-S or the pyridonol-O) takes up the proton, while the metal ion itself acts as a Lewis acid in the heterolytic cleavage of H_2, prior to hydride transfer to methenyl-H_4MPT^+.[20,36−38,40,41] This work shows that an alternative scenario might be feasible, in which the metal ion acts as a proton acceptor and gets formally oxidized during the reaction. This work also demonstrates that superelectrophilic activation by protonation, which has been proposed for methenyl-H_4MPT^+ to increase its carbocationic character,[70−72] is not necessarily required for an imidazolinium ion to serve as a hydride acceptor. Our ongoing studies aim for improving both FLP components in such bioinspired systems, for using these metalate-based FLPs also for the activation of other small molecules, and for answering the question whether catalytic reactions are possible.

EXPERIMENTAL SECTION

General Considerations. All reactions were carried out under argon (dried over phosphorus pentoxide on solid support and liberated from traces of oxygen by a heated copper catalyst) using standard Schlenk techniques or in a glovebox (MBRAUN LabMaster) under a nitrogen atmosphere. Solvents were dried and degassed by standard procedures before use. Hydrogen gas was purchased from Messer, and deuterium gas was provided by Linde. **KRp** and its polymeric form **Rs** were synthesized as described previously.[48] The syntheses of $[^{Tol}Im^{Mes}]^+Br^-$ and $[^{Mes}Im^{F4}]^+Br^-$ are described in the Supporting Information. NMR spectra were recorded on Bruker Avance 300 or 500 instruments at 25 °C if not noted otherwise. Chemical shifts (δ) are given in ppm and are referenced to the solvent residual signals.[73] The peaks are labeled according to their splitting patterns with s (singlet), d (doublet), t (triplet), q (quartet), quin (quintet), or m (multiplet). ^{19}F NMR spectra were referenced externally relative to $CFCl_3$. Reactions which required high pressures of H_2 or D_2 were performed in Wilmad-LabGlass high-pressure NMR tubes (medium wall, 524-PV-7). Mass spectrometry was performed on an Applied Biosystems API 2000 device or on a Bruker HCTultra instrument. IR spectra were recorded using either an Excalibur FTS 3000 spectrometer or a Cary 630 FTIR spectrometer (Agilent) equipped with DialPath accessory and placed in a glovebox (MBRAUN UNIlab, argon atmosphere). IR bands were labeled according to their relative intensities with vs (very strong), s (strong), m (medium), w (weak), and very weak (vw).

Computational Details. Calculations concerning the mechanism of dihydrogen splitting by the FLP $Rp^-/[^{Tol}Im^{F4}]^+$ were carried out with the ORCA program package.[74] The B3LYP functional[61] was used including dispersion corrections as proposed by Grimme et al.,[75] with Becke−Johnson damping.[76] The basis sets used were the def2-SVP, def2-TZVP, and def2-QZVPP sets,[62] in combination with the respective Stuttgart/Dresden effective core potential ECP.[77] The RIJCOSX approximation was used throughout in order to accelerate the calculation of two-electron integrals.[78] All structure optimizations were carried out in the gas phase. The thermodynamic corrections used to derive the Gibbs free energies (as well as the zero point energy) were based on harmonic frequency calculations considering a temperature of 298.15 K. In order to correct for solution effects, single points with the COSMO continuum model were performed with standard defaults for MeCN (ε = 36.6).[63] The Rp^- anion as well as the imidazolinium ion $[^{Tol}Im^{F4}]^+$ were optimized at the B3LYP-D3/def2-TZVP level of theory.

The free energies were further corrected to take into account the loss of translational degrees of freedom in solution. The latter strongly impacts reaction steps in which the number of educt and product molecules changes. According to the cell model of Ardura et al.,[64] the ideal gas computed free energy for a bimolecular reaction A + B → A − B should be corrected by:

$$\Delta\Delta G_{sol} = RT\ln[v_c(A)v_c(B)/v_c(A-B)] - RT\ln[k_BT/p] \quad (1)$$

In the case of a trimolecular process, one will have

$$\Delta\Delta G_{sol} = RT\ln[v_c(A)v_c(B)v_c(C)/v_c(A-B-C)] - 2RT\ln[k_BT/p] \quad (2)$$

where v_c corresponds to the cavity volume from the continuum model, and R, k_B, T, and p, correspond to the ideal gas and Boltzmann constants, temperature, and pressure, respectively. This results in corrections of −13.8 (bimolecular) and −32.6 kJ mol^{-1} (trimolecular) for the reaction steps considered, since the reference state corresponds to three separated molecular units (H_2, Rp^- and $[^{Tol}Im^{F4}]^+$).

In order to obtain the Lewis pair, the compounds were placed in close contact. The ruthenium complex was then rotated about the axis of contact to obtain starting structures for geometry optimization. The Gibbs free energy was computed for each resulting local minimum. The final electronic energy was computed at the B3LYP-D3/def2-QZVPP level, including a COSMO correction from single point calculations with the def2-TZVP basis set to simulate the influence of the surrounding solvent MeCN. This procedure was followed in all other stationary points of the reaction path. In order to follow the hydrogen dissociation at the site, a H_2 molecule was added in varying positions around the C−Ru bridge in the dimer and optimized. For each structure obtained, reaction paths were obtained by placing a harmonic potential along a predefined reaction coordinate (difference between the C−H and H−H distances) and optimizing the structure under this constraint (0.5 Bohr stepsize and a 0.1 hartree/Bohr^2 force constant). The reaction path calculations, due to the large number of combinations tried, were carried out with the smaller def2-SVP basis set.

Crystal Structure Determination. X-ray data were collected on a STOE IPDS II diffractometer with an area detector (graphite monochromated Mo−Kα radiation, λ = 0.71073 Å) by use of ω scans at 133 K (see Table S1 for crystal data and refinement details). The structures were solved by direct methods (SHELXS-97) and refined on F^2 using all reflections with SHELXL-97 ($[^{Tol}Im^{F4}]^+Br^-$ and $H^{Tol}Im^{F4}$) or SHELXL-2013 ($[Rp^{Tol}Im^{F3}]^+Br^-$).[79] Non-hydrogen atoms were refined anisotropically. Most hydrogen atoms were placed in calculated positions and assigned to an isotropic displacement parameter of 1.2/1.5 U_{eq}(C). A fixed isotropic displacement parameter of 0.08 Å^2 was applied in case of the oxygen bound hydrogen atoms (H_2O) in $[^{Tol}Im^{F4}]^+Br^-$ as well as two DFIX restraints (d_{O-H} = 0.82 Å). Face-indexed absorption corrections were performed numerically with the program X-RED.[80] CCDC-944125 ($[^{Tol}Im^{F4}]^+Br^-$), CCDC-944126 ($H^{Tol}Im^{F4}$), and CCDC-1007089 ($[Rp^{Tol}Im^{F3}]^+Br^-$) contain the supplementary crystallographic data for this paper. These data can be obtained free of charge from The Cambridge Crystallographic Data Centre via http://www.ccdc.cam.ac.uk/data_request/cif.

Synthesis of *N,N′*-Bis(2,6-difluorophenyl)-4-tolu-amidine. *N,N′*-Bis(2,6-difluorophenyl)-4-toluamidine was synthesized according to modified existing protocols.[81,82] Diphosphorus pentoxide (21.3 g, 75.0 mmol, 6.0 equiv), hexamethyldisiloxane (26.0 g, 34.2 mL, 160 mmol, 13 equiv), and dichloromethane (30 mL) were heated to reflux for 1 h. All volatile compounds were removed by distillation at 160 °C. To the obtained viscous syrup *p*-toluic acid (1.70 g, 12.5 mmol, 1.0 equiv) and 2,6-difluoroaniline (4.06 g, 3.39 mL, 31.4 mmol, 2.5 equiv) were added, and the mixture was heated to 160 °C for 44 h. The hot reaction mixture was poured into aqueous KOH solution (0.5 M, 400 mL), stirred for 30 min, and extracted with dichloromethane (3 × 200 mL). The combined organic extracts were dried over Na_2SO_4,

dx.doi.org/10.1021/ja509186d | J. Am. Chem. Soc. 2014, 136, 16626−16634

concentrated in vacuo, and filtered over neutral aluminum oxide. *N*-pentane was then added to the solution, and the mixture was kept at −26 °C to induce crystallization. Filtration and washing the product with *n*-pentane afforded the amidine as colorless crystals (3.83 g, 10.7 mmol, 86%). The compound exists as a mixture of two isomers in solution (ratio approximately 3:1 under the applied conditions). This gives rise to a rather complicated NMR spectrum, which has been observed for other amidines before.[83] For reasons of clarity, only the NMR data of the main isomer are given here. ^{1}H NMR (500 MHz, $CDCl_3$, 223 K): δ (ppm) = 7.31 (d, ^3J(H,H) = 8 Hz, 2 H; *o*-Tol-H), 7.16−7.07 (m, 3 H; *p*-Ar-H, *m*-Tol-H), 6.94 (dd, ^3J(H,F) = 9 Hz, ^3J(H,H) = 7 Hz, 2 H; *m*-Ar-H), 6.78−6.67 (m, 3 H; *p*-Ar-H, *m*-Ar-H), 6.64 (s, 1 H; NH), 2.28 (s, 3 H; CH_3). ^{13}C NMR (126 MHz, $CDCl_3$, 223 K): δ (ppm) = 159 (C-2), 157 (dd, ^1J(C,F) = 265 Hz, ^3J(C,F) = 6 Hz; *o*-Ar-C), 155 (dd, ^1J(C,F) = 260 Hz, ^3J(C,F) = 6 Hz; *o* -Ar-C), 141 (*p*-Tol-C), 130 (*ipso*-Tol-C), 129 (*m*-Tol-C), 128 (t, ^2J(C,F) = 16 Hz; *ipso*-Ar-C), 128 (*o*-Tol-C), 126 (t, ^3J(C,F) = 9 Hz; *p*-Ar-C), 122 (t, ^{3} J(C,F) = 9 Hz; *p*-Ar-C), 116 (t, ^2J(C,F) = 16 Hz; *ipso*-Ar-C), 112 (dd, ^2J(C,F) = 20 Hz, ^4J(C,F) = 3 Hz; *m*-Ar-C), 111 (dd, ^2J(C,F) = 18 Hz, ^4J(C,F) = 5 Hz; *m*-Ar-C), 22 (CH_3). ^{19}F NMR (282 MHz, $CDCl_3$): δ (ppm) = −120 (s, 2 F; Ar-F), −122 (s, 2 F; Ar-F). IR (KBr): $\tilde{\nu}$(cm^{-1}) = 3409 (m), 3192 (w), 2954 (w), 2913 (w), 2363 (w), 1643 (s), 1607 (s), 1524 (m), 1509 (m), 1468 (s), 1385 (w), 1328 (m), 1312 (m), 1288 (m), 1274 (m), 1240 (m), 1183 (w), 1150 (w), 1105 (w), 1058 (w), 1005 (s), 948 (w), 928 (w), 862 (w), 816 (m), 781 (m), 734 (m), 722 (m), 686 (w), 654 (w), 630 (w), 590 (w), 568 (w), 530 (w), 505 (w), 486 (m). MS (ESI$^+$, MeCN): *m*/*z* (%) = 359.1 (100) [M + H]$^+$.

Synthesis of 1,3-Bis(2,6-difluorophenyl)-2-(4-tolyl)-imidazolinium Bromide ([^{Tol}Im^{F4}]$^+$Br$^-$). *N*,*N*′-Bis(2,6-difluorophenyl)-4-toluamidine (1.0 g, 2.8 mmol) and 1,2-dibromoethane (5 mL) were heated to reflux for 52 h. The solvent was removed in vacuo, and the crude product was dissolved in dichloromethane (15 mL). After washing with saturated $NaHCO_3$ solution (15 mL) and drying over Na_2SO_4, the organic phase was concentrated. Upon addition of Et_2O, the product precipitated as a beige solid which can be recrystallized from DCM/Et_2O (0.33 g, 0.71 mmol, 25%). Since half of the amount of utilized amidine serves as a base in this reaction, the maximum yield is 50%. After precipitation of the product, the organic phase still contains *N*,*N*′-bis(2,6-difluorophenyl)-4-toluamidine, which can be reused for additional runs of the reaction. ^{1}H NMR (300 MHz, CD_3CN): δ (ppm) = 7.60−7.50 (m, 2 H; *p*-Ar-H), 7.21−7.10 (m, 8 H; *m*-Ar-H, Tol-H), 4.67 (s, 4 H, CH_2), 2.27 (s, 3 H; CH_3). ^{13}C NMR (75 MHz, CD_3CN): δ (ppm) = 170.2 (C-2), 158.7 (dd, ^1J(C,F) = 254 Hz, ^3J(C,F) = 3 Hz; *o*-Ar-C), 147.3 (*p*-Tol-C), 134.1 (t, ^3J(C,F) = 10 Hz; *p*-Ar-C), 131.0 (*m*-Tol-C), 129.2 (*o*-Tol-C), 118.3 (*ipso*-Tol-C), 114.3 (t, ^2J(C,F) = 16 Hz; *ipso*-Ar-C), 113.9 (dd, ^2J(C,F) = 19 Hz, ^4J(C,F) = 4 Hz; *m*-Ar-C), 53.2 (CH_2), 21.7 (CH_3). ^{19}F{^{1}H} NMR (282 MHz, CD_3CN): δ (ppm) = −118.5 (s, 4 F; Ar-F). IR (KBr): $\tilde{\nu}$(cm^{-1}) = 3057 (w), 2907 (vw), 2051 (vw), 1603 (m), 1582 (s), 1544 (s), 1475 (s), 1369 (w), 1295 (m), 1236 (m), 1190 (m), 1050 (m), 1004 (s), 804 (m), 789 (s), 723 (w), 561 (m), 517 (m). IR (CD_3CN): $\tilde{\nu}$ (cm^{-1}) = 2230 (w), 2107 (w), 1625 (w), 1605 (m), 1586 (s), 1556 (s), 1484 (vs), 1376 (w), 1305 (m), 1251 (w), 1015 (m), 827 (w), 797 (m), 728 (w). MS (ESI$^+$, MeCN): *m*/*z* (%) = 385.0 (100) [M−Br]$^+$. MS (ESI$^-$, MeCN): *m*/*z* (%) = 79 (100) [Br]$^-$.

Synthesis of 1,3-bis(2,6-difluorophenyl)-2-(4-tolyl)-imidazolidine (H^{Tol}Im^{F4}). To a solution of [^{Tol}Im^{F4}]$^+$Br$^-$ (60 mg, 0.13 mmol, 1.0 equiv) in EtOH (10 mL) $NaBH_4$ (7.2 mg, 0.19 mmol, 1.5 equiv) was added in small portions, and the mixture was stirred at room temperature for 2 h. The solvent was removed in vacuo. After addition of $CHCl_3$, the resulting suspension was filtered (Sartorius PTFE syringe filter, 0.45 μm) and again concentrated. By this procedure imidazolidine H^{Tol}Im^{F4} was obtained quantitatively as determined by NMR spectroscopy. ^{1}H NMR (300 MHz, CD_3CN): δ (ppm) = 7.23 (d, ^3J(H,H) = 8 Hz, 2 H; *o*-Tol-H), 7.00−6.78 (m, 8 H; Ar-H, *p*-Tol-H), 6.07 (quin, ^5J(H,F) = 2 Hz, 1 H; CH), 4.09−3.97 (m, 2 H; CH_2), 3.64−3.52 (m, 2 H; CH_2), 2.18 (s, 3 H; CH_3). ^{13}C NMR (75 MHz, CD_3CN): δ (ppm) = 159.9 (dd, ^1J(C,F) = 247 Hz, ^3J(C,F) = 7 Hz; *o*-Ar-C), 139.3 (*p*-Tol-C), 138.7 (*ipso*-Tol-C), 129.5 (*m*-Tol-C), 128.9 (*o*-Tol-C), 125.1 (t, ^3J(C,F) = 10 Hz; *p*-Ar-C), 123.8 (t, ^2J(C,F) = 14 Hz; *ipso*-Ar-C), 113.0 (dd, ^2J(C,F) = 17 Hz, ^4J(C,F) = 8 Hz; *m*-Ar-C), 80.0 (quin, ^4J(C,F) = 4 Hz; CH), 51.3 (t, ^4J(C,F) = 3 Hz; CH_2), 21.1 (CH_3). ^{19}F{^{1}H} NMR (282 MHz, CD_3CN): δ (ppm) = −120.3 (s, 4 F; Ar-F). IR (CD_3CN): $\tilde{\nu}$(cm^{-1}) = 1619 (w), 1590 (w), 1571 (w), 1495 (s), 1474 (s), 1351 (m), 1305 (w), 1290 (m), 1230 (m), 1180 (w), 1162 (w), 1068 (w), 1000 (m), 843 (w), 828 (w), 782 (m), 722 (w).

Synthesis of 1,3-Bis(2,6-difluorophenyl)-2-(4-tolyl)-(2−2H)-imidazolidine (D^{Tol}Im^{F4}). The compound was prepared analogously to imidazolidine H^{Tol}Im^{F4}, but instead of $NaBH_4$ deuterated $NaBD_4$ (8.0 mg, 0.19 mmol, 1.5 equiv) was used. By this procedure imidazolidine D^{Tol}Im^{F4} was obtained quantitatively as determined by NMR spectroscopy. ^{1}H NMR (300 MHz, CD_3CN): δ (ppm) = 7.23 (d, ^3J(H,H) = 8 Hz, 2 H; *o*-Tol-H), 6.99−6.78 (m, 8 H; Ar-H, *p*-Tol-H), 4.09−3.98 (m, 2 H; CH_2), 3.63−3.52 (m, 2 H; CH_2), 2.18 (s, 3 H; CH_3). ^{13}C NMR (75 MHz, CD_3CN): δ (ppm) = 159.9 (dd, ^1J(C,F) = 247 Hz, ^3J(C,F) = 8 Hz; *o*-Ar-C), 139.3 (*p*-Tol-C), 138.6 (*ipso*-Tol-C), 129.5 (*m*-Tol-C), 128.9 (*o*-Tol-C), 125.0 (t, ^3J(C,F) = 10 Hz; *p*-Ar-C), 123.8 (t, ^2J(C,F) = 14 Hz; *ipso*-Ar-C), 113.0 (dd, ^2J(C,F) = 17 Hz, ^4J(C,F) = 8 Hz; *m*-Ar-C), 80.1−79.2 (m; CD), 51.3 (t, ^4J(C,F) = 3 Hz; CH_2), 21.1 (CH_3). ^{19}F{^{1}H} NMR (282 MHz, CD_3CN): δ (ppm) = −120.4 (s, 4 F; Ar-F). IR (CD_3CN): $\tilde{\nu}$(cm^{-1}) = 1571 (w), 1619 (w), 1586 (w), 1497 (s), 1474 (s), 1344 (m), 1290 (m), 1232 (m), 1160 (w), 1147 (w), 1085 (w), 1003 (m), 977 (w), 828 (w), 784 (m), 722 (w).

Adduct formation between [Im^{F4}]$^+$Br$^-$ and KRp ([Rp^{Tol}Im^{F3}]$^+$Br$^-$). [^{Tol}Im^{F4}]$^+$Br$^-$ (70 mg, 0.15 mmol, 1.0 equiv) and **KRp** (39 mg, 0.15 mmol, 1.0 equiv) were dissolved in MeCN (10 mL) and stirred at room temperature. The reaction was largely complete after 5 h as determined by IR spectroscopy (see Supporting Information); besides traces of the dimer **Rp$_2$** ($\tilde{\nu}$(CO) = 1996, 1775 cm^{-1}) only the adduct [Rp^{Tol}Im^{F3}]$^+$ was detected in solution. The resulting suspension was filtered (Sartorius PTFE syringe filter, 0.45 μm), and the solvent was removed under reduced pressure. The remaining solid was then washed with small amounts of THF and toluene and dissolved in MeCN. Layering toluene with the MeCN solution produced—upon standing at room temperature—crystals suitable for X-ray crystallography confirming the identity of the adduct [Rp^{Tol}Im^{F3}]$^+$Br$^-$. ^{1}H NMR (500 MHz, CD_3CN): δ (ppm) = 7.55−7.49 (m, 1 H; *p*-Ar-H), 7.35 (ddd, ^{3} J(H,H) = 8 Hz, ^4J(H,H) = 1 Hz, ^5J(H,F) = 1 Hz, 1 H; *m*- **Rp** Ar-H), 7.25−7.12 (m, 5 H; *m*-Ar-H, Tol-H), 7.05−7.01 (m, 1 H; *m*-Ar-H), 6.94 (td, ^3J(H,H) = 8 Hz, ^4J(H,F) = 6 Hz, 1 H; *p*-**Rp**Ar-H), 6.72 (ddd, ^3J(H,F) = 10 Hz, ^3J(H,H) = 8 Hz, ^4J(H,H) = 1 Hz, 1 H; *m*-**Rp**Ar-H), 5.54 (s, 5 H; Cp), 4.87−4.81 (m, 1 H; CH_2), 4.72−4.66 (m, 1 H; CH_2), 4.60−4.53 (m, 1 H; CH_2), 4.40−4.33 (m, 1 H; CH_2), 2.24 (s, 3 H; CH_3). ^{13}C{^{1}H} NMR (126 MHz, CD_3CN): δ (ppm) = 202.6 (CO), 201.0 (CO), 169.9 (C-2), 159.3 (dd, ^1J(C,F) = 254 Hz, ^3J(C,F) = 3 Hz; *o*-Ar-C), 158.6 (d, ^1J(C,F) = 252 Hz; *o*-**Rp**Ar-C), 158.3 (dd, ^1J(C,F) = 254 Hz, ^3J(C,F) = 3 Hz; *o*-Ar-C), 146.6 (*p*-Tol-C), 145.2 (s_{br}; *o*-**Rp**Ar-C), 144.1 (d, ^4J(C,F) = 4 Hz; *m*-**Rp**Ar-C), 134.6 (d, ^2J(C,F) = 9 Hz; *ipso*-**Rp**Ar-C), 133.7 (t, ^3J(C,F) = 10 Hz; *p*-Ar-C), 130.6 (*m*-Tol-C), 129.5 (*o*-Tol-C), 129.0 (d, ^3J(C,F) = 8 Hz; *p*-**Rp**Ar-C), 119.1 (*ipso*-Tol-C), 114.7 (t, ^2J(C,F) = 16 Hz; *ipso*-Ar-C), 113.9 (t, ^2J(C,F) = 20 Hz; *m*-Ar-C), 113.8 (t, ^2J(C,F) = 20 Hz; *m*-Ar-C), 112.1 (d, ^2J(C,F) = 20 Hz; *m*-**Rp**Ar-C), 91.0 (Cp), 53.8 (CH_2), 52.6 (CH_2), 21.6 (CH_3). ^{19}F NMR (471 MHz, CD_3CN): δ (ppm) = −118.4−(−118.5) (m, 1 F; *o*-Ar-F), −118.9−(−118.9) (m, 1 F; *o*-Ar-F), −119.5−(−119.5) (m, 1 F; *o*-**Rp**Ar-F). IR (CD_3CN): $\tilde{\nu}$ (cm^{-1}) = 2034 (s), 1971 (s). MS (ESI$^+$, MeCN): *m*/*z* (%) = 589.1 (100) [M]$^+$.

Reactions of [^{Tol}Im^{F4}]$^+$Br$^-$ and the Black Solid Rs with H_2/D_2. The black solid **Rs** (11 mg, equivalent to 0.04 mmol/1.4 equiv **KRp**[84]) was transferred to a high pressure NMR tube (Wilmad-LabGlass) in the glovebox. After addition of [^{Tol}Im^{F4}]$^+$Br$^-$ (14 mg, 0.030 mmol, 1.0 equiv) dissolved in CD_3CN/CH_3CN (0.6 mL), the sample was immediately frozen (N_2) and degassed by repeated freeze−thaw cycles. Addition of H_2 or D_2 (8 bar) was followed by warming to room temperature. In order to guarantee a sufficient mixing of the heterogeneous solution, the sample was placed in an ultrasonic bath

dx.doi.org/10.1021/ja509186d | J. Am. Chem. Soc. 2014, 136, 16626−16634

equipped with a timer (2 min on, 12 min off). By this method, an undesired heating of the bath is avoided, and room temperature is maintained throughout the reaction.

■ ASSOCIATED CONTENT

Supporting Information

Supplemental figures described in the text; ^{1}H, ^{19}F, and ^{2}H NMR spectra; IR spectra; crystallographic details; synthetic details for imidazolium ions $[^{Tol}Im^{Mes}]^{+}Br^{-}$ and $[^{Mes}Im^{F4}]^{+}Br^{-}$; details of the reaction of **KFp** with $[^{Tol}Im^{F4}]^{+}Br^{-}$. This material is available free of charge via the Internet at http://pubs.acs.org.

■ AUTHOR INFORMATION

Corresponding Author

franc.meyer@chemie.uni-goettingen.de

Notes

The authors declare no competing financial interest.

■ ACKNOWLEDGMENTS

Financial support by the DFG (International Research Training Group GRK 1422 "Metal Sites in Biomolecules: Structures, Regulation and Mechanisms") and the Fonds der Chemischen Industrie (Ph.D. fellowship for K.F.K.) is gratefully acknowledged.

■ REFERENCES

(1) Mazloomi, K.; Gomes, C. *Renewable Sustainable Energy Rev.* **2012**, *16*, 3024−3033.
(2) Andrews, J.; Shabani, B. *Procedia Eng.* **2012**, *49*, 15−25.
(3) Alper, J. *Science* **2003**, *299*, 1686−1687.
(4) Thauer, R. K. *Eur. J. Inorg. Chem.* **2011**, *7*, 919−921.
(5) Dawson, J.; Ghiotto, F.; McMaster, J.; Schroeder, M. In *Molecular Solar Fuels, RSC Energy and Environment Series No. 5*; Wydrzynski, T. J., Hillier, W., Eds.; Royal Society of Chemistry: Cambridge, U.K.2012; pp 326−386.
(6) Lubitz, W.; Ogata, H.; Reijerse, E.; Higuchi, Y. In *Molecular Solar Fuels, RSC Energy and Environment Series No. 5*; Wydrzynski, T. J., Hillier, W., Eds.; Royal Society of Chemistry: Cambridge, U.K., 2012; pp 288−325.
(7) Lubitz, W.; Ogata, H.; Rüdiger, O.; Reijerse, E. *Chem. Rev.* **2014**, *114*, 4081−4148.
(8) Lubitz, W.; Reijerse, E.; van Gastel, M. *Chem. Rev.* **2007**, *107*, 4331−4365.
(9) De Lacey, A. L.; Fernandez, V. M.; Rousset, M.; Cammack, R. *Chem. Rev.* **2007**, *107*, 4304−4330.
(10) Fontecilla-Camps, J. C.; Volbeda, A.; Cavazza, C.; Nicolet, Y. *Chem. Rev.* **2007**, *107*, 4273−4303.
(11) Siegbahn, P. E. M.; Tye, J. W.; Hall, M. B. *Chem. Rev.* **2007**, *107*, 4414−4435.
(12) Simmons, T. R.; Berggren, G.; Bacchi, M.; Fontecave, M.; Artero, V. *Coord. Chem. Rev.* **2014**, *270*−*271*, 127−150.
(13) Wang, M.; Chen, L.; Li, X.; Sun, L. *Dalton Trans.* **2011**, *40*, 12793−12800.
(14) Ohki, Y.; Tatsumi, K. *Eur. J. Inorg. Chem.* **2011**, 973−985.
(15) Gloaguen, F.; Rauchfuss, T. B. *Chem. Soc. Rev.* **2009**, *38*, 100−108.
(16) Tard, C.; Pickett, C. J. *Chem. Rev.* **2009**, *109*, 2245−74.
(17) Shima, S.; Thauer, R. K. *Chem. Rec.* **2007**, *7*, 37−46.
(18) Shima, S.; Ermler, U. *Eur. J. Inorg. Chem.* **2011**, 963−972.
(19) Corr, M. J.; Murphy, J. A. *Chem. Soc. Rev.* **2011**, *40*, 2279−2292.
(20) Dey, S.; Das, P. K.; Dey, A. *Coord. Chem. Rev.* **2013**, *257*, 42−63.
(21) Zirngibl, C.; Hedderich, R.; Thauer, R. K. *FEBS Lett.* **1990**, *261*, 112−116.
(22) Thauer, R. K.; Klein, A. R.; Hartmann, G. C. *Chem. Rev.* **1996**, *96*, 3031−3042.
(23) Shima, S.; Pilak, O.; Vogt, S.; Schick, M.; Stagni, M. S.; Meyer-Klaucke, W.; Warkentin, E.; Thauer, R. K.; Ermler, U. *Science* **2008**, *321*, 572−575.
(24) Hiromoto, T.; Ataka, K.; Pilak, O.; Vogt, S.; Stagni, M. S.; Meyer-Klaucke, W.; Warkentin, E.; Thauer, R. K.; Shima, S.; Ermler, U. *FEBS Lett.* **2009**, *583*, 585−590.
(25) Wright, J. A.; Turrell, P. J.; Picket, C. J. *Organometallics* **2010**, *29*, 6146−6156.
(26) Hiromoto, T.; Warkentin, E.; Moll, J.; Ermler, U.; Shima, S. *Angew. Chem., Int. Ed.* **2009**, *48*, 6457−6460.
(27) Schultz, K. M.; Chen, D.; Hu, X. *Chem.—Asian J.* **2013**, *8*, 1068−1075.
(28) Chen, D.; Scopelliti, R.; Hu, X. *J. Am. Chem. Soc.* **2010**, *132*, 928−929.
(29) Hu, B.; Chen, D.; Hu, X. *Chem.—Eur. J.* **2014**, *20*, 1677−1682.
(30) Turrell, P. J.; Wright, J. A.; Peck, J. N. T.; Oganesyan, V. S.; Pickett, C. J. *Angew. Chem., Int. Ed.* **2010**, *49*, 7508−7511.
(31) Turrell, P. J.; Hill, A. D.; Ibrahim, S. K.; Wright, J. A.; Pickett, C. J. *Dalton Trans.* **2013**, *42*, 8140−8146.
(32) Royer, A. M.; Salomone-Stagni, M.; Rauchfuss, T. B.; Meyer-Klaucke, W. *J. Am. Chem. Soc.* **2010**, *132*, 16997−17003.
(33) Chen, D.; Scopelliti, R.; Hu, X. *Angew. Chem., Int. Ed.* **2011**, *50*, 5671−5673.
(34) Song, L.-C.; Xie, Z.-J.; Wang, M.-M.; Zhao, G.-Y.; Song, H.-B. *Inorg. Chem.* **2012**, *51*, 7466−7468.
(35) Song, L.-C.; Zhao, G.-Y.; Xie, Z.-J.; Zhang, J.-W. *Organometallics* **2013**, *32*, 2509−2512.
(36) Yang, X.; Hall, M. B. *J. Am. Chem. Soc.* **2008**, *130*, 14036−14037.
(37) Yang, X.; Hall, M. B. *J. Am. Chem. Soc.* **2009**, *131*, 10901−10908.
(38) Dey, A. *J. Am. Chem. Soc.* **2010**, *132*, 13892−13901.
(39) Stiebitz, M. T.; Reiher, M. *Inorg. Chem.* **2010**, *49*, 5818−5823.
(40) Finkelmann, A. R.; Striebitz, M. T.; Reiher, M. *J. Phys. Chem. B* **2013**, *117*, 4806−4817.
(41) Finkelmann, A. R.; Senn, H. M.; Reiher, M. *Chem. Sci.* **2014**, *5*, 4474−4482.
(42) Welch, G. C.; San Juan, R. R.; Masuda, J. D.; Stephan, D. W. *Science* **2006**, *314*, 1124−1126.
(43) Stephan, D. W.; Erker, G. *Angew. Chem., Int. Ed.* **2010**, *49*, 46−76.
(44) Erker, G.; Stephan, D. W. *Top. Curr. Chem.* **2013**, *332*, 1−350.
(45) Holschumacher, D.; Bannenberg, T.; Hrib, C. G.; Jones, P. G.; Tamm, M. *Angew. Chem., Int. Ed.* **2008**, *47*, 7428−7432.
(46) Chase, P. A.; Stephan, D. W. *Angew. Chem., Int. Ed.* **2008**, *47*, 7433−7437.
(47) Estes, D. P.; Vannucci, A. K.; Hall, A. R.; Lichtenberger, D. L.; Norton, J. R. *Organometallics* **2011**, *30*, 3444−3447.
(48) Kalz, K. F.; Kindermann, N.; Xiang, S.-Q.; Kronz, A.; Lange, A.; Meyer, F. *Organometallics* **2014**, *33*, 1475−1479.
(49) Owen, G. R. *Chem. Soc. Rev.* **2012**, *41*, 3535−3546.
(50) Harman, W. H.; Peters, J. C. *J. Am. Chem. Soc.* **2012**, *134*, 5080−5082.
(51) Podiyanachari, S. K.; Fröhlich, R.; Daniliuc, C. G.; Petersen, J. L.; Mück-Lichtenfeld, C.; Kehr, G.; Erker, G. *Angew. Chem., Int. Ed.* **2012**, *51*, 8830−8833.
(52) Podiyanachari, S. K.; Kehr, G.; Mück-Lichtenfeld, C.; Daniliuc, C. G.; Erker, G. *J. Am. Chem. Soc.* **2013**, *135*, 17444−17456.
(53) Fong, H.; Moret, M.-E.; Lee, Y.; Peters, J. C. *Organometallics* **2013**, *32*, 3053−3062.
(54) Bauer, J.; Braunschweig, H.; Dewhurst, R. D.; Radacki, K. *Chem.—Eur. J.* **2013**, *19*, 8797−8805.
(55) Jiang, Y.; Blacque, O.; Fox, T.; Berke, H. *J. Am. Chem. Soc.* **2013**, *135*, 7751−7760.
(56) Chapman, A. M.; Haddow, M. F.; Wass, D. F. *J. Am. Chem. Soc.* **2011**, *133*, 18463−18478.
(57) Wass, D. F.; Chapman, A. M. *Top. Curr. Chem.* **2013**, *334*, 261−280.

(58) Sgro, M. J.; Stephan, D. W. *Angew. Chem., Int. Ed.* **2012**, *51*, 11343−11345; *Angew. Chem.* **2012**, *124*, 11505−11507.
(59) Flynn, S. R.; Wass, D. F. *ACS Catal.* **2013**, *3*, 2574−2581.
(60) Bartoschek, S.; Buurman, G.; Thauer, R. K.; Geierstanger, B. H.; Weyrauch, J. P.; Griesinger, C.; Nilges, M.; Hutter, M. C.; Helms, V. *ChemBioChem* **2001**, *2*, 530−541.
(61) Becke, A. D. *J. Chem. Phys.* **1993**, *98*, 5648−5652.
(62) Weigend, F.; Ahlrichs, R. *Phys. Chem. Chem. Phys.* **2005**, *7*, 3297−3305.
(63) Klamt, A.; Schürmann, G. *J. Chem. Soc. Perkin Trans. 2* **1993**, 799−805.
(64) Ardura, D.; López, R.; Sordo, T. L. *J. Phys. Chem. B* **2005**, *109*, 23618−23623.
(65) Reiher, M.; Hess, B. A. *Chem.—Eur. J.* **2002**, *8*, 5332−5339.
(66) Using an ultrasonic bath, just like in the reactions with H_2/D_2 (see Experimental Section), over a period of 2 days to finely disperse the solid material **Rs** resulted in the gradual decomposition of the imidazolinium salt $[^{Tol}\mathbf{Im}^{F4}]^+$. While 67% of the initial imidazolinium salt remained unchanged in solution under these conditions, the reaction mixture also contained an undefined product showing two resonances in the ^{19}F NMR spectrum at −120 and −131 ppm (not observed in the presence of H_2/D_2), but only trace amounts of the imidazolidine $\mathbf{H}^{Tol}\mathbf{Im}^{F4}$. Adding trace amounts of water to the reaction mixture before the ultrasonic bath treatment leads to an increase of the amount of the undefined reaction product. The origin of the trace amounts of imidazolidine $\mathbf{H}^{Tol}\mathbf{Im}^{F4}$ formed in these control experiments, in the absence of H_2/D_2, could not be finally clarified. Possible sources of the hydride ion could be a contamination of the material **Rs** with the borohydride, which is used in the synthesis of **Rs**,[48] or traces of an alternative hydride source in the material **Rs**.
(67) Davison, A.; McCleverty, J. A.; Wilkinson, G. *J. Chem. Soc.* **1963**, 1133−1138.
(68) Moore, E. J.; Sullivan, J. M.; Norton, J. R. *J. Am. Chem. Soc.* **1986**, *108*, 2257−2263.
(69) Gubler, J.; Finkelmann, A. R.; Reiher, M. *Inorg. Chem.* **2013**, *52*, 14205−14215.
(70) Berkessel, A.; Thauer, R. K. *Angew. Chem., Int. Ed. Engl.* **1995**, *34*, 2247−2250.
(71) Berkessel, A. *Curr. Opin. Chem. Biol.* **2001**, *5*, 486−490.
(72) Corr, M. J.; Gibson, K. F.; Kennedy, A. R.; Murphy, J. A. *J. Am. Chem. Soc.* **2009**, *131*, 9174−9175.
(73) Fulmer, G. R.; Miller, A. J. M.; Sherden, N. H.; Gottlieb, H. E.; Nudelman, A.; Stoltz, B. M.; Bercaw, J. E.; Goldberg, K. I. *Organometallics* **2010**, *29*, 2176−2179.
(74) Neese, F. *WIREs Comput. Mol. Sci.* **2012**, *2*, 73−78.
(75) Grimme, S.; Antony, J.; Ehrlich, S.; Krieg, H. *J. Chem. Phys.* **2010**, *132*, 154104/1−154104/19.
(76) Grimme, S.; Ehrlich, S.; Goerigk, L. *J. Comput. Chem.* **2011**, *32*, 1456−1465.
(77) Andrae, D.; Häußermann, U.; Dolg, M.; Stoll, H.; Preuß, H. *Theor. Chim. Acta* **1990**, *77*, 123−141.
(78) Neese, F.; Wennmohs, F.; Hansen, A.; Becker, U. *Chem. Phys.* **2009**, *356*, 98−109.
(79) Sheldrick, G. M. *Acta Crystallogr.* **2008**, *A64*, 112−122.
(80) *X-RED*; STOE & CIE GmbH: Darmstadt, Germany, 2002.
(81) Ogata, S.; Mochizuki, A.; Kakimoto, M.; Imai, Y. *Bull. Chem. Soc. Jpn.* **1986**, *59*, 2171−2177.
(82) Bambirra, S.; Otten, E.; van Leusen, D.; Meetsma, A.; Hessen, B. *Z. Anorg. Allg. Chem.* **2006**, *632*, 1950−1952.
(83) Häfelinger, G.; Kuske, K. H. In *The Chemistry of Amidines and Imidates*; Patai, S., Rappoport, Z., Eds.; Wiley: Chichester, U.K., 1991; Vol. 2.
(84) The exact structure and formula weight of the black solid **Rs** are unclear. Equivalents were therefore calculated assuming a molecular weight identical to **KRp** to get a rough impression of the required amount of black material.